Eva Kiss*, Stefan Kins, Karin Gorgas, Maret Orlik, Carolin Fischer, Kristina Endres, Andrea Schlicksupp, Joachim Kirsch and Jochen Kuhse*

Artemisinin-treatment in pre-symptomatic APP-PS1 mice increases gephyrin phosphorylation at Ser270: a modification regulating postsynaptic $GABA_AR$ density

https://doi.org/10.1515/hsz-2021-0153
Received February 17, 2021; accepted March 29, 2021; published online April 20, 2021

Abstract: Artemisinins, a group of plant-derived sesquiterpene lactones, are efficient antimalarial agents. They also share anti-inflammatory and anti-viral activities and were considered for treatment of neurodegenerative disorders like Alzheimer's disease (AD). Additionally, artemisinins bind to gephyrin, the multifunctional scaffold of GABAergic synapses, and modulate inhibitory neurotransmission *in vitro*. We previously reported an increased expression of gephyrin and $GABA_A$ receptors in early pre-symptomatic stages of an AD mouse model (APP-PS1) and in parallel enhanced CDK5-dependent phosphorylation of gephyrin at S270. Here, we studied the effects of artemisinin on gephyrin in the brain of young APP-PS1 mice. We detected an additional increase of gephyrin protein level, elevated gephyrin phosphorylation at Ser270, and an increased amount of $GABA_AR$-γ2 subunits after artemisinin-treatment. Interestingly, the CDK5 activator p35 was also upregulated. Moreover, we demonstrate decreased density of postsynaptic gephyrin and $GABA_AR$-γ2 immunoreactivities in cultured hippocampal neurons expressing gephyrin with alanine mutations at two CDK5 phosphorylation sites. In addition, the activity-dependent modulation of synaptic protein density was abolished in neurons expressing gephyrin lacking one or both of these phosphorylation sites. Thus, our results reveal that artemisinin modulates expression as well as phosphorylation of gephyrin at sites that might have important impact on GABAergic synapses in AD.

Keywords: APP-PS1; artemisinin; GABA(A)-ergic synapses; gephyrin phosphorylation; p35.

Present address: **Maret Orlik**, Koordinierungszentrum für Klinische Studien, University of Heidelberg, Heidelberg, Germany.
Carolin Fischer, Department of Neurology and Epileptology, Hertie Institute for Clinical Brain Research, University of Tübingen, Tübingen, Germany.

***Corresponding authors: Eva Kiss**, Institute of Anatomy and Cell Biology, University of Heidelberg, Im Neuenheimer Feld 307, D-69120 Heidelberg, Germany; and Department of Cellular and Molecular Biology, University of Medicine, Pharmacy, Science and Technology "G.E. Palade" of Târgu Mures, Str. Gheorghe Marinescu nr. 38, 540 139 Târgu Mureș, Romania, E-mail: kiss@ana.uni-heidelberg.de and **Jochen Kuhse**, Institute of Anatomy and Cell Biology, University of Heidelberg, Im Neuenheimer Feld 307, D-69120 Heidelberg, Germany, E-mail: jochen.kuhse@urz.uni-heidelberg.de. https://orcid.org/0000-0002-4140-0487
Stefan Kins, Department of Human Biology and Human Genetics, University of Kaiserslautern, 67633 Kaiserslautern, Germany, E-mail: s.kins@biologie.uni-kl.de
Karin Gorgas, Maret Orlik, Carolin Fischer, Andrea Schlicksupp and Joachim Kirsch, Institute of Anatomy and Cell Biology, University of Heidelberg, Im Neuenheimer Feld 307, D-69120 Heidelberg, Germany, E-mail: Gorgas@ana.uni-heidelberg.de (K. Gorgas), Maret.Orlik@med.uni-heidelberg.de (M. Orlik), carolin.fischer@uni-tuebingen.de (C. Fischer), schlicksupp@ana.uni-heidelberg.de (A. Schlicksupp), joachim.kirsch@urz.uni-heidelberg.de (J. Kirsch)
Kristina Endres, Department of Psychiatry and Psychotherapy, University Medical Center Johannes Gutenberg-University Mainz, 55131 Mainz, Germany, E-mail: kristina.endres@unimedizin-mainz.de

Introduction

Alzheimer's disease (AD) is the most common cause of dementia characterized by progressive loss of memory affecting an increasing number of persons worldwide. Efforts to find curative treatments for AD patients mostly failed so far. This can be assigned at least partially to the still incompletely clarified pathogenesis of the disease and delayed start of therapies (Frozza et al. 2018). Mutations in the amyloid precursor protein (APP) and enzymes involved in its processing, e.g., presenilin 1 (PS1) resulting in increased levels of Aβ, were identified as causes of the autosomal dominant, early-onset familial form of AD. The etiology and neurobiological processes that lead to sporadic AD (about 95% of AD cases) are still not completely understood. For a long time, research has been focused on

Aβ plaque and neurofibrillary tangle pathology, the morphological hallmarks of AD, but meanwhile increasing evidence indicates the soluble forms of Aβ to play a central role in AD-pathogenesis, evoking increased inflammation, mitochondrial failure, disruption of Ca^{++}-homeostasis or deregulation of protein posttranslational modifications (Selkoe and Hardy 2016). All of these processes can represent a link to the impairments of different forms of synaptic plasticity which apparently develop long before the onset of clinical symptoms of AD (Zott et al. 2018).

Hyperactivation of cyclin dependent kinase 5 (CDK5), a proline-directed serine/threonine kinase with broad range roles in the development and homeostasis of the central nervous system (Mishiba et al. 2014), seems to intervene at various levels in the pathogenesis of AD and was even proposed as potential target for AD therapy (Shupp et al. 2017). In addition to causing aberrant hyperphosphorylation of tau and neurofilament proteins as well as of APP and PS1 (Liu et al. 2016), CDK5 deregulation is considered to contribute substantially to the altered synaptic plasticity in AD (Hawasli et al. 2007) affecting memory formation and behavior (Mishiba et al. 2014). For excitatory synapses, CDK5-dependent signaling was shown to regulate neurotransmitter release (Kim and Ryan 2010), dendritic spine density (Mita et al. 2016), and postsynaptic N-methyl-D-aspartate (NMDA) receptor clustering (Hawasli et al. 2007), the latter being dependent on the phosphorylation of the major scaffold protein of the excitatory synapses postsynaptic density protein 95 (PSD-95) (Morabito et al. 2004). However, information about putative CDK5-dependent structural and functional changes of inhibitory GABAergic synapses and their role in AD are sparse.

We recently reported Aβ-dependent elevation of the protein levels of CDK5 and p35, a major regulatory protein of CDK5 in the hippocampus of young presymptomatic APP-PS1 mice, accompanied by increased phosphorylation of gephyrin (Kiss et al. 2016, 2020). Gephyrin is the major scaffold protein of inhibitory synapses which anchors $GABA_A$Rs at postsynaptic membrane specializations and was shown to be regulated by different posttranslational modifications, including phosphorylation (Groeneweg et al. 2018). Interestingly, we found that the elevated phosphorylation at Ser270, a CDK5-dependent phosphorylation site within the linker domain of gephyrin correlated to increased $GABA_A$ receptor γ2 ($GABA_A$R-γ2) subunit expression (Hollnagel et al. 2019; Kiss et al. 2020). This indicates that APP/Aβ has a profound impact on inhibitory network properties already early in the disease progression, and that these effects may be at least partially mediated by p35/CDK5 phosphorylation of gephyrin.

At present, it is largely accepted that in addition to excitatory synapses the inhibitory GABAergic system also undergoes significant remodeling in the AD-brain and intervene in the regulation of the neuronal pathways involved in memory and learning (Kwakowsky et al. 2018; Vico et al. 2019). Remarkably, treatment of two transgenic models with dihydromyricetin, a positive allosteric modulator of $GABA_A$Rs, ameliorated behavioral deficits and reversed neuropathology in aged transgenic mice to some extent by reducing Aβ peptide concentrations and restoring gephyrin levels (Liang et al. 2014). Thus, a better understanding of inhibition especially in early pathogenesis of AD appears to be crucially important holding the promise that modulating the GABAergic system along the development of AD might be therapeutically relevant (Calvo-Flores Guzmán et al. 2018).

The anchoring of $GABA_A$ receptors (as well as inhibitory glycine receptors [GlyR]) at inhibitory synapses is mediated by a lattice formed by gephyrin underneath the plasma membrane due to the multimerization capacity of this protein (Kneussel et al. 1999; Specht et al. 2013). Gephyrin is composed of structured N-terminal G-domains and C-terminal E-domains connected via an intrinsic disordered central linker region (Prior et al. 1992). A receptor-binding pocket located in the E-domain mediates the binding of gephyrin to the large intracellular loop of GlyR β and $GABA_A$ receptors (Kim et al. 2006; Maric et al. 2011).

Interestingly, a low molecular mass organic compound, the membrane permeable sesquiterpene artemisinin, derived from the sweet wormwood plant *Artemisia annua*, has been recently identified to competitively bind to this receptor-anchoring pocket of the E-domain of gephyrin (Kasaragod et al. 2019). Consequently, this binding was proposed to reduce $GABA_A$ receptor-anchoring and thus its density at postsynaptic membrane specializations. However, in non-neuronal cells treatment with artemether led to an elevated gephyrin expression and GABAergic signaling (Li et al. 2017). Moreover, several recent publications reported that artemisinin and its derivatives effectively reduce amyloid plaque load and neuroinflammation in mouse models of AD (Ho et al. 2014; Qiang et al. 2018; Zhao et al. 2020).

To gain insights into the putative regulation of gephyrin expression and GABAergic synapses by artemisinin in neuronal tissue *in vivo* (while avoiding amyloid plaque related changes), we analyzed the expression of inhibitory synapse proteins in young APP-PS1 mice that were treated for six weeks with two different doses of

artemisinin. Using immunoblot and immunofluorescence (IF) microscopy analyses we detected an increase in the level of gephyrin, gephyrin phosphorylation at Ser270, and $GABA_AR$-γ2 as well as p35 in the hippocampus of artemisinin-treated APP-PS1 mice. Site-directed mutagenesis of gephyrin at Ser270 and/or Ser200, another putative CDK5 phosphorylation site in cultured primary hippocampus neurons, provided evidence for the functional impact of the phosphorylation at these sites for the activity-dependent clustering of gephyrin and γ2-$GABA_A$ receptor subunits at postsynaptic membrane specializations. Thus, the treatment with artemisinin fostered the probably Aβ-induced early increase of the p35/CDK5-dependent gephyrin phosphorylation in young APP-PS1 mice potentially affecting GABAergic inhibitory synapses in this model of cerebral amyloidosis.

Results

Treatment of young APP-PS1 mice with artemisinin increases gephyrin and p35 protein levels and results in elevated gephyrin phosphorylation at Ser270

In earlier studies we detected a significant increase of gephyrin and other key inhibitory synapse proteins in the hippocampus of three-month-old APP-PS1 mice (Hollnagel et al. 2019; Kiss et al. 2016, 2020) indicating altered GABAergic inhibition already in the early phase of AD-like pathogenesis.

Based on the recently reported findings showing a direct link between gephyrin and the potentially neuroprotective artemisinins (Qiang et al. 2018) with both positive (Li et al. 2017) and negative (Kasaragod et al. 2019) modulation of GABAergic signaling *in vitro*, we treated APP-PS1 mice with artemisinin to test its possible modulatory effects on the inhibitory drive in the AD-brain. Six-week-old APP-PS1 mice were fed for six weeks with artemisinin-containing diet (10 and 100 mg/kg) and analyzed for the expression of gephyrin at three months of age, when in the hippocampus amyloid plaques are not yet developed (Kiss et al. 2016; Radde et al. 2006).

We first performed Western blot analysis of hippocampus homogenates prepared in parallel with tissue samples used for immunostaining and IF-microscopic analyses. The genotype of the APP-PS1 mice was demonstrated by the robust expression of hAPP (Figure 1). As shown in Figure 1, the level of gephyrin detected with a pan-gephyrin antibody was increased in the hippocampus homogenates of artemisinin-treated APP-PS1 mice in a concentration-dependent manner, eliciting significant increase with the dose of 100 mg/kg ($p < 0.01$) (Figure 1B). Interestingly, the signal intensity detected with the phospho-sensitive gephyrin antibody (mAb7a) was significantly elevated with 10 mg/kg artemisinin (Figure 1B, C), suggesting that the phosphorylation of gephyrin at Ser270 may be fostered predominately upon low doses of artemisinin. In earlier studies we have shown that gephyrin is phosphorylated by CDK5/p35 *in vitro* (Kalbouneh 2013; Kalbouneh et al. 2014; Kuhse et al. 2012) and demonstrated an increased expression of p35 in the hippocampus of young APP-PS1 mice (Kiss et al. 2020). Therefore, we subsequently analyzed the protein levels of p35. Although the quantification of the specific p35 WB bands did not delivered statistically significant differences between groups, p35 protein levels in the hippocampus homogenates of low dose artemisinin-treated mice were constantly increased in comparison to samples from untreated animals (Figure 1).

Next we performed IF-staining of coronal cryosections cut from fresh-frozen brains using in addition to the phospho-specific anti-gephyrin (mAb7a) and anti-p35 antibodies also an antibody directed against the $GABA_AR$-γ2 subunits to prove whether a putative change in the gephyrin phosphorylation might coincide with changes of another functionally relevant inhibitory synaptic protein. The labeling with all three antibodies generated a similar distribution in all experimental groups and confirmed our earlier observations in three-month-old APP-PS1 mice (Kiss et al. 2016, 2020): a rather intense gephyrin, $GABA_AR$-γ2 and p35 immunoreactivity in the somata of neurons of pyramidal (CA1) and granular cells of dentate gyrus (DG) (Figure 2A, C, E). Brightly stained mostly punctate structures were also observed, probably representing the clustered postsynaptic proteins distributed across the dendritic layers of hippocampus (insets) (Figure 2A, C, E). As shown in Figure 2, the analysis of immunolabeled brain sections confirmed the increase of mAb7a and p35 immunoreactivities in the hippocampus of artemisinin-treated mice in comparison to non-treated APP-PS1 mice, and in addition revealed also an increase of $GABA_AR$-γ2 subunit immunoreactivity. The quantification of mean IF-intensities in CA1 and DG of the hippocampus in contrast to the Western blot analysis of whole hippocampus homogenates detected a significant increase also for p35 in these hippocampal subregions of artemisinin-treated APP-PS1 mice (Figure 2B, D, F). This finding in addition to the lack of clear-cut differences between low and high dose induced changes in the sub-regional level of these proteins suggested possible dose- and region-dependent differences in their regulation

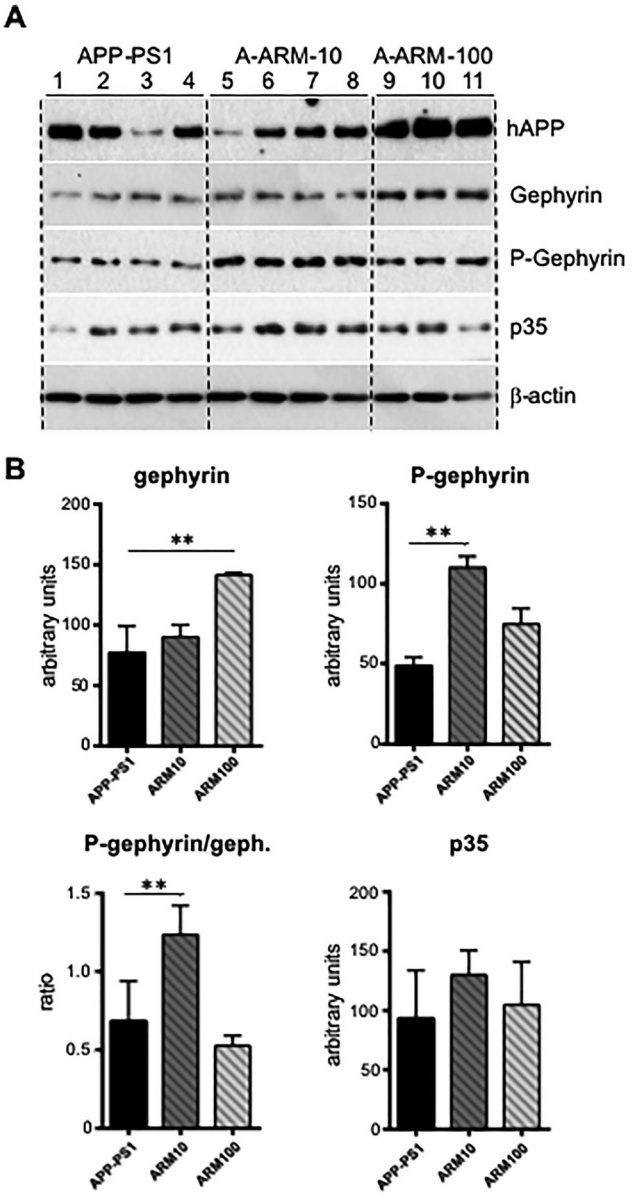

Figure 1: Artemisinin fosters gephyrin protein level and gephyrin phosphorylation in hippocampus homogenates of three-month-old APP-PS1 mice.
(A) Representative immunoblots of hippocampus lysates obtained from three-month-old APP-PS1 mice, untreated (APP-PS1) or treated with two doses of artemisinin, 10 mg/kg (A-ARM10) or 100 mg/kg (A-ARM100) and probed with a pan anti-gephyrin (Gephyrin), the phospho-specific anti-gephyrin mAb7a (P-Gephyrin), and an anti-p35 antibody. The antibody against the human transgenic APP (hAPP) was used to verify the genotype, and a mouse anti β-actin antibody was used as a loading control. (B) Quantification of protein band intensities shown in A for gephyrin, phospho-gephyrin and p35; phospho-gephyrin normalized to gephyrin protein is also shown. Note the significant increase of gephyrin protein level with 100 mg/kg artemisinin, whereas gephyrin phosphorylation level was fostered especially in hippocampus extracts from mice treated with 10 mg/kg artemisinin; band intensities were quantified from 3–4 mice/group. Student's *t*-test. Means ± SD, $^{**}p < 0.01$.

by artemisinins. However, the detected increase in the IF-intensity of all three proteins was evidently more consistent at the lower dose of 10 mg/kg than at 100 mg/kg, thus showing a consensus with the Western blot data (Figure 1).

These results indicate that artemisinin especially at low dose exerts an obvious effect on p35 expression and possibly a subsequent increase of gephyrin phosphorylation at the CDK5-dependent phosphorylation site Ser270 in the hippocampus of young APP-PS1 mice with potential consequences on $GABA_A$ receptor and inhibitory synapse remodeling. Thus, we decided to study the relevance of this CDK-dependent phosphorylation site of gephyrin as a potential player in mediating effects of artemisinin on inhibitory synapses.

Myc-tagged gephyrin is particularly suitable to study the role of CDK5-dependent phosphorylation sites in gephyrin and $GABA_A$ receptor clustering

To investigate, whether the phosphorylation of gephyrin at Ser270 detected by mAb7a might be functionally involved in gephyrin and $GABA_A$ receptor clustering, a lentivirus shRNA knockdown approach was established to reduce effectively the endogenous gephyrin expression in cultured hippocampal neurons. We tested two different gephyrin-knockdown shRNA sequences targeting the gephyrin mRNA 3′UTR sequence. The suitability of shRNA1 for this purpose is demonstrated in Supplementary Figure 1. Control hippocampal neurons displayed a high number of somatic and dendritic gephyrin clusters at DIV14, while after infection with shRNA1 expressing lentiviruses (pFSGW-Geph-Kd1) at DIV6, the number, size, and IF-intensities of mAb7a positive immunoreactive puncta was reduced significantly (e.g., the cluster number from 18.68 ± 0.6 to 1.56 ± 0.63) (mean ± standard error of the mean [SEM]) ($p < 0.001$) (Supplementary Figure 1A, B), attesting that infection of hippocampal neurons with viruses expressing shRNA1 has an efficient "knockdown" effect on gephyrin cluster formation and is suitable for the analysis of the phenotype by gephyrin mutated at specific phosphorylation sites. For this purpose, we used a mEos2-gephyrin fusion construct (Specht et al. 2013), a mutated mEos2-gephyrin^{S270A} or another N-terminally myc-tagged gephyrin cloned into pFSGW-Geph-Kd1 (see Materials and Methods).

The fluorescence of recombinant mEos2-gephyrin protein in addition to enlarged dendritic puncta revealed

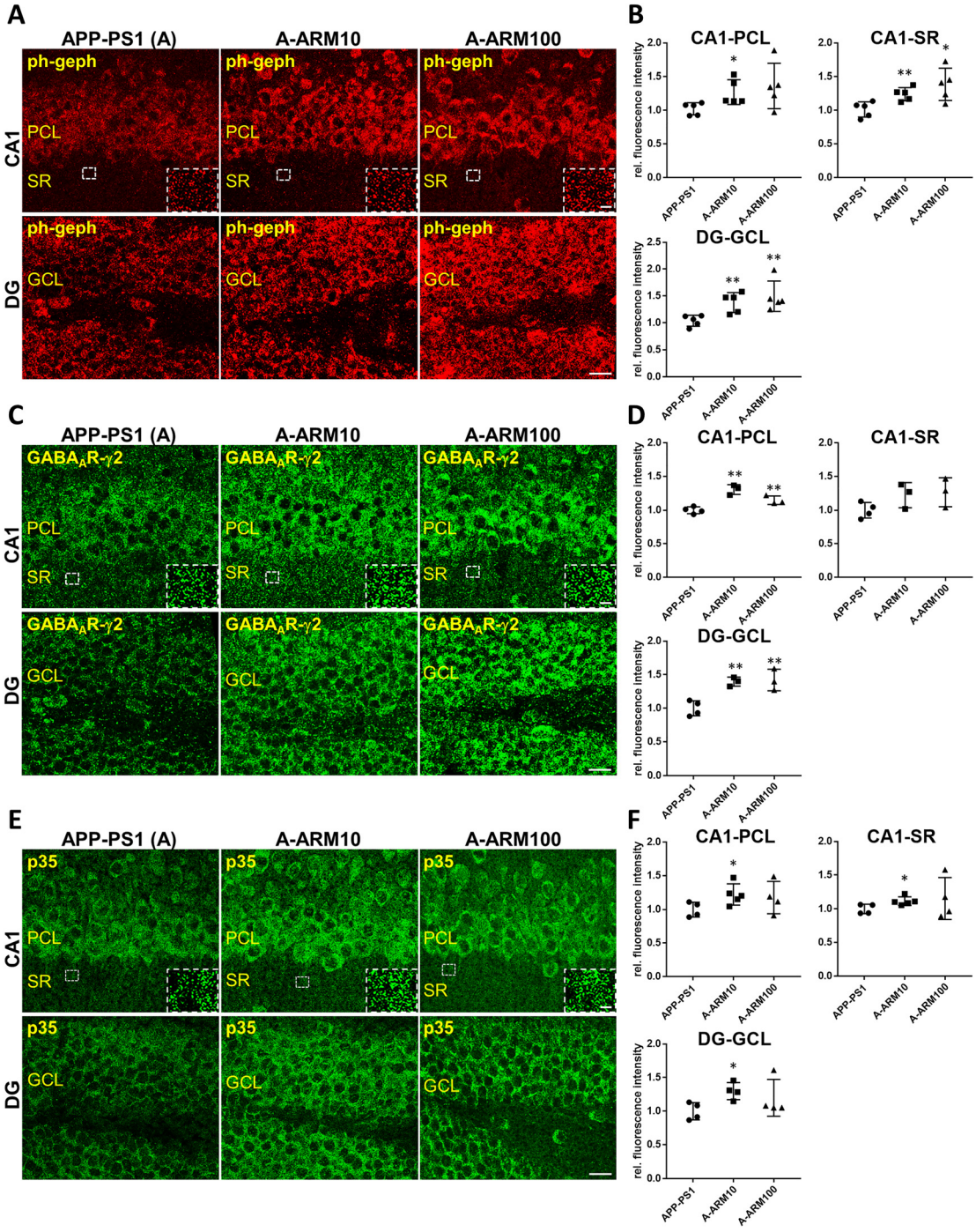

Figure 2: Gephyrin phosphorylation at Ser270, as well as GABA$_A$R-γ2 and p35 immunreactivity is increased in hippocampal sub-regions of three-month-old APP-PS1 mice after artemisinin-treatment.

Representative IF images demonstrating increased intensity of mAb7a (A), GABA$_A$R-γ2 (C) and p35 (E) immunoreactivities within the CA1 and dentate gyrus (DG) of the hippocampus of three-month-old APP-PS1 mice treated with two doses of artemisinin, 10 mg/kg (A-ARM10) and 100 mg/kg (A-ARM100). Insets show positive labeled clusters within the stratum radiatum (SR) of the CA1 region. Note the more intense somatic labeling of all three proteins in the neurons of the pyramidal cell layer (PCL) of CA1 and granular cell layer (GCL) of the DG in comparison to probably predominant dendritic segments in SR for all experimental groups. Confocal maximum intensity projection images (four optical sections, 2 µm thick Z-stack). Scale bars: 100 µm; insets: 10 µm. (B) Quantification of mean IF-intensities (see Methods) for mAb7a (D) GABA$_A$R-γ2 and (F) p35 measured in randomly selected regions of interest in the PLC and SR of CA1 and the GCL of DG from Z-stacks of eight optical section images (one optical section: 500 nm) confirming the significantly higher fluorescence intensity levels in hippocampal sections of APP-PS1 mice after treatment with artemisinin. n = 3–6 animals/group; Means ± SEM; *p < 0.05, **p < 0.01; Student's t-test.

larger somatic perinuclear mEos2-gephyrin aggregates in most of the cells (Supplementary Figure 1). Number, size and intensity of clustered mEos2-gephyrin^{S270A} fluorescence in proximal dendrites of 20 infected neurons from four independent cultures were slightly increased without significant differences (Supplementary Figure 1C–F). The observation of perinuclear mEos2-gephyrin aggregates indicated that the large N-terminal Eos2-fusion protein might interfere with the assembly process of gephyrin that is governed by the trimerization of the N-terminal gephyrin G-domain (Saiyed et al. 2007) possibly hindering an efficient analysis of the phenotype of gephyrin mutants, an observation that might be relevant as a large number of publication used N-terminal GFP-gephyrin fusion proteins for functional analysis *in vitro* and *in vivo*.

Therefore, we used for further analysis myc-tagged gephyrin which displayed staining patterns very similar to that of the endogenously expressed gephyrin of control cells (Supplementary Figure 1G, H) and revealed an efficient expression in gephyrin-knockdown cells.

Expression of recombinant myc-gephyrin harboring alanine substitutions at two putative CDK5-dependent phosphorylation sites reduces the synaptic density of gephyrin and GABA$_A$R-γ2 subunits

Next we tested the functional impact of the phosphorylation at Ser270 by introduction of an alanine codon at this position within the myc-gephyrin reading frame. We analyzed the mutant myc-Gephyrin^{S270A} expressed in cultured hippocampal neurons by IF microscopy after triple staining using anti-myc, anti-GABA$_A$R-γ2 and anti-VIAAT antibodies, the latter detecting the presynaptic vesicular inhibitory amino acid transporters. In addition, we included in our analysis another gephyrin mutant with an alanine substitution at Ser200 (myc-Gephyrin^{S200A}), which is localized within another CDK5-consensus sequence (SPHK) and was shown in earlier studies to be phosphorylated by CDK5 *in vitro* (Kalbouneh 2013) as well as a gephyrin mutant carrying both substitutions (myc-Gephyrin^{S200A,S270A}). The number, size and average fluorescence intensity of clustered myc-gephyrin and GABA$_A$R-γ2-subunits and VIAAT were analyzed. Interestingly, the number and size of gephyrin puncta were not significantly different comparing wild-type and the three different mutant myc-gephyrin proteins (Supplementary Figure 2). Importantly, when measuring the average IF-intensities at the overlapping colocalization areas of the three proteins a significant reduction of gephyrin and GABA$_A$R-γ2 immunoreactivity was detected with the two single mutants analyzed, whereas no synergistic effect of the double mutation (myc-gephyrin^{S200A,S270A}) on these parameters could be observed (Figure 3). The VIAAT-IF-intensity in this overlay area was less affected by the gephyrin mutations (Figure 3D), although a tendency to reduced mean values was also observed. Thus, our results suggest that phosphorylation of gephyrin at both CDK5-dependent sites may contribute to the density of gephyrin within the postsynaptic scaffold lattice determining directly or indirectly the density of γ2-subunit harboring GABA$_A$ receptors.

Activity-dependent changes of GABA$_A$R-γ2 subunits are affected by alanine substitution-mutations of putative CDK5 phosphorylation sites

Next we asked whether the phosphorylation of gephyrin at Ser200 and Ser270 might be important for activity-dependent inhibitory synapse remodeling. For this scope, we used gabazine to block the activity of GABA$_A$ receptors since this dumping of tonic inhibition allows synchronous action potential bursting which is mediated by glutamatergic synaptic transmission (Arnold et al. 2005).

First, we analyzed whether the lentiviral infection causing down-regulation of endogenous gephyrin and its replacement by recombinant myc-gephyrin protein allows the same burst-activation effect of gabazine as in control cultures. We recorded the oscillating burst activity by measuring the changes of fluorescence of the Ca^{++}-sensitive protein hSyn:GCaMP6f.NLS.HA, that was co-expressed with the recombinant gephyrin. The quantification of the frequency of nuclear calcium transients (see Material and Methods) revealed that in cell cultures expressing myc-gephyrin, oscillations were efficiently induced with 5 μM gabazine bath application, very similar to the control cultures (Supplementary Figure 3A). More interestingly, in cells expressing myc-gephyrin^{S270A}, maximal frequency of nuclear calcium transients was induced already with 10 times lower gabazine concentrations (0.5 μM) than in cells expressing wild-type myc-gephyrin, suggesting a decreased inhibitory drive by myc-gephyrin^{S270A}. Thus, these experiments supported the hypothesis that gephyrin Ser270 is functionally important for GABAergic transmission.

For further analysis, we fixed cells after a bath perfusion of 5 μM gabazine for 5 h, then triple stained them by

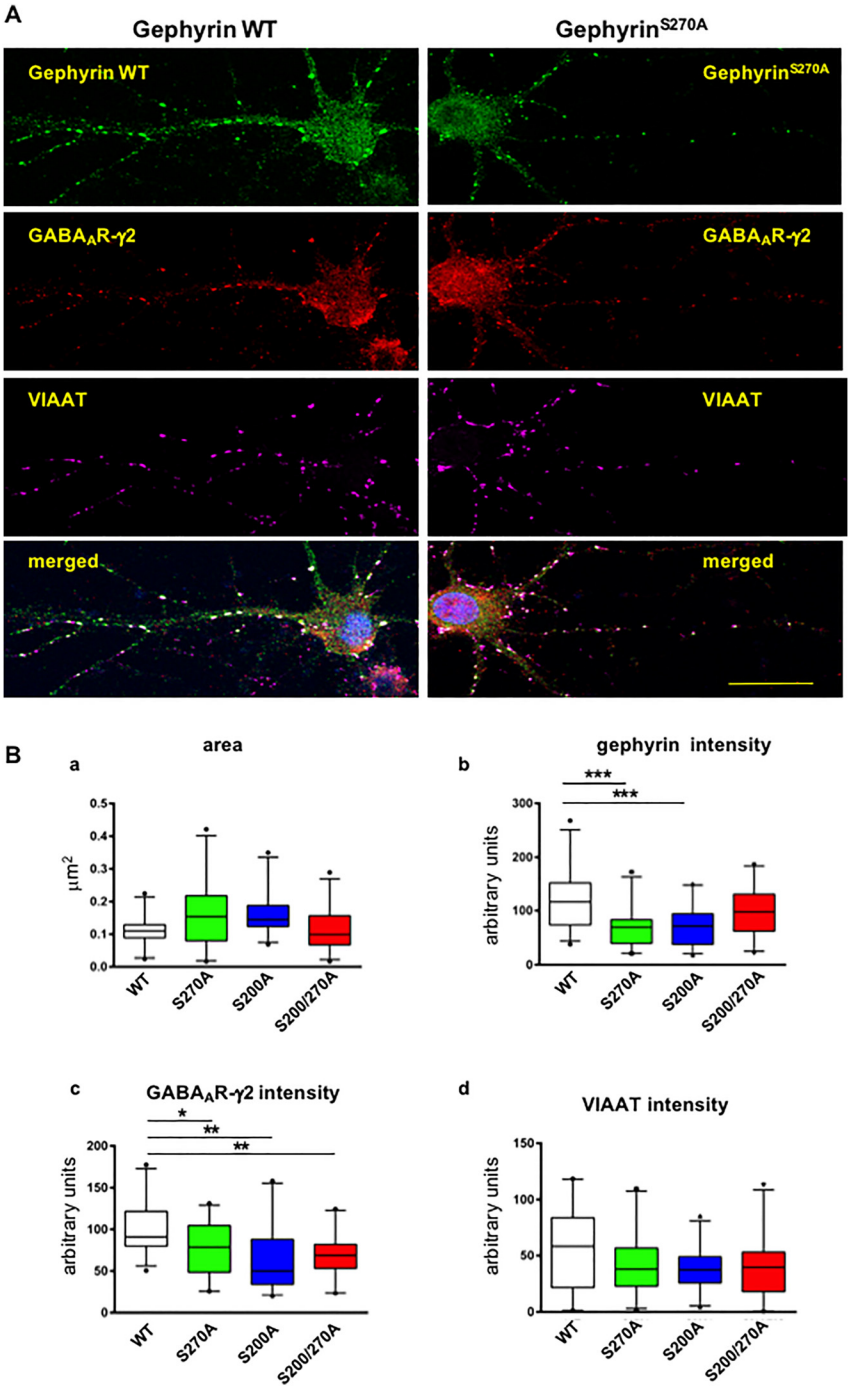

Figure 3: Alanine substitutions at gephyrin AA S200 or S270 reduce density of postsynaptic immunoreactivities of myc-gephyrin and GABA$_A$R-γ2 subunit clusters in hippocampal neurons.
(A) Representative IF-microscopy images reveal a large degree of overlapping immunoreactivities specific for transiently expressed recombinant WT myc-gephyrin (left panel) (green), GABA$_A$ receptor γ2 (red) and VIAAT (magenta), or gephyrin mutant myc-gephyrin^{S270A} (right panel). Scale bar: 20 µm. (B) Quantification of area (a) and IF-intensities of gephyrin (b), GABA$_A$R-γ2 (c) VIAAT (d) at postsynaptic sites identified as overlapping signals colored in green, red and magenta. Results for gephyrin^{Ser270A} (green), gephyrin^{S200A} (blue) and gephyrin^{Ser200AS270A} (red) compared to wild-type gephyrin (white). Cluster immunoreactivities were quantified at proximal dendritic segments (25 µm length) of 25 cells derived from four independent cultures. Scale bar: 20 µm. The median of values is shown with box-plots with 10th and 90th percentile. One-way ANOVA with Tukey's post-hoc test. *$p < 0.05$; **$p < 0.001$; ***$p < 0.0001$.

using anti-myc, anti-GABA$_A$R-γ2 and anti-VIAAT antibodies and analyzed the average fluorescence intensities at the colocalized and overlapping synaptic areas by confocal fluorescence microscopy. As shown in Figure 4, the inhibition of GABA$_A$ receptor activity with gabazine decreased the density of postsynaptic gephyrin and GABA$_A$R-γ2 subunits at synapses in cells harboring wild-type gephyrin. However, in neurons expressing gephyrin that lost one of the putative CDK5 phosphorylation sites, the activity-dependent change of synaptic protein density was abolished (see Figure 4C). Surprisingly, the density of synaptic GABA$_A$R-γ2 subunits in cells expressing the double mutant myc-gephyrin^{S200A,S270A} was increased upon inhibition of GABA$_A$ receptor activity with gabazine. Thus, the level of phosphorylation on both sites of gephyrin might be important to determine synergistically the receptor density at postsynaptic membrane specializations dependent on the synaptic activity.

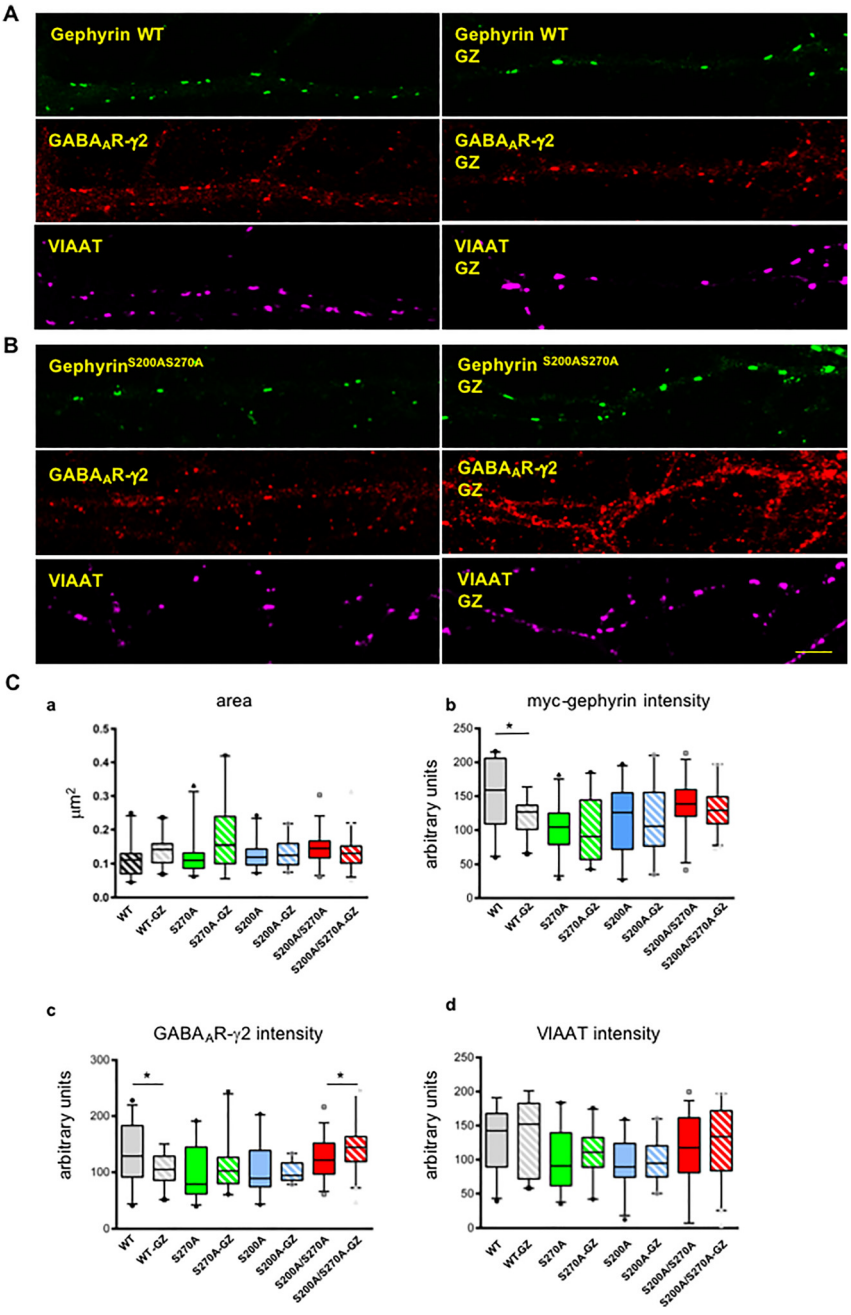

Figure 4: Decreased density of postsynaptic myc-gephyrin and GABA$_A$R-γ2 subunit cluster-immunoreactivities in hippocampal neurons upon receptor inhibition with 5 μM gabazine.
(A) Typical pattern of immunoreactivities for transiently expressed recombinant myc-gephyrin (green), GABA$_A$R-γ2 subunit (red), and VIAAT (magenta), and (B) mutated recombinant gephyrin (S200A, S270A) which is also co-localized with GABA$_A$R-γ2 clusters in hippocampal neurons under steady-state (left side) and gabazine inhibition (GZ) (right side) conditions. Scale bar: 5 μm. (C) The areas of overlaps (AOLs) did not change significantly between gephyrin wild-type and mutants neither under steady-state nor gabazine inhibition conditions (a). Expression of wild-type gephyrin (gray) revealed reduction of average gephyrin (b) and GABA$_A$R-γ2 (c) IF-intensities in AOLs upon receptor inhibition with gabazine for 5 h (GZ), whereas expression of gephyrin with alanine substitutions at one CDK site (Ser270, green) or (Ser200, blue) prohibited these gabazine induced changes. However, with both sites mutated (gephyrin^{Ser200AS270A}, red) an increase of average IF-intensity for GABA$_A$R-γ2 was observed in AOLs upon gabazine inhibition. Average IF-intensity in AOLs for VIAAT (d) did not change significantly comparing steady state and gabazine (GZ) inhibition (5 h) conditions for either WT nor gephyrin mutants. Cluster immunoreactivities were estimated for proximal dendritic segments of 20 μm length from 25–40 cells derived from three independent cultures. The median of values is shown with box-plots with 10th and 90th percentile. Students' *t*-test. *$p < 0.05$.

Discussion

The data presented here provide novel information about the *in vivo* effects of artemisinin, a plant-derived multi-potent drug in an AD mouse model. We demonstrate in the hippocampus of young pre-plaque stage APP-PS1 mice, which were treated with artemisinin, a significant elevation of gephyrin phosphorylation at a CDK5/p35-dependent site Ser270, and that the increased phosphorylation of gephyrin correlates on the one hand with an increased expression of the CDK5 regulatory protein p35 and on the other hand with a higher abundance of the γ2 subunits of GABA$_A$ receptors. In addition, we deliver *in vitro* data which support the detected *in vivo* effects of artemisinin in the hippocampus of pre-symptomatic APP-PS1 mice, by indicating a functionally relevant route for the modulation of inhibitory synapses by this drug.

Several recent studies proposed artemisinins as potential drugs for the treatment of AD reducing amyloid plaque load and neuroinflammation in different mouse models (for review see Lu et al. 2019; Seo et al. 2018). In the brain of five-month-old APPswe/PS1dE9 mice artemisinin-

treatment was shown to inhibit NF-κB activity and NALP3 inflammasome activation (Shi et al. 2013). This finding was supported by an additional study identifying also NF-κB and a Nrf2-dependent mechanisms mediating the anti-inflammatory effects of artemether in BV2 microglia (Okorji et al. 2016). More recent studies demonstrated also an improvement of learning and memory in AD mouse models mainly correlating with the suppressed neuroinflammation by artemisinins (Li et al. 2019; Qiang et al. 2018; Zhao et al. 2020). Interestingly, in the latter study by Zhao et al., some neuroprotective effects of artemisinin were attributed to the phosphorylation of ERK1/2 and CREB as demonstrated in SH-SY5Y cells (Zhao et al. 2020). However, *in vivo* data concerning putative alterations of excitatory or inhibitory synaptic connectivity in the brain, which may be induced by treatment with artemisinins, are largely missing.

Gephyrin was identified as a target of artemisinins in a screen for drugs improving insulin secretion in pancreatic islet cells. In this study, artemether, one of several types of sequesterterpene lactones, collectively termed artemisinins, was shown to increase insulin secretion in α-cells of the pancreas, which was dependent on gephyrin stabilization and enhanced GABAergic signaling (Li et al. 2017). In fact, it was shown that the expression of the $GABA_AR$-γ2 subunit was increased on both the mRNA and protein levels upon artemether-treatment in these cells. In another recent study, an artemisinin binding site within the gephyrin E-domain was characterized demonstrating a competitive binding of artemisinins and the M3-M4 intracellular loop of the glycine receptor (GlyR) β-subunit to the gephyrin binding pocket in the E-domain (Kasaragod et al. 2019). Here, the competitive binding of artemisinin, artemether and artesunate was shown to reduce binding and thus surface expression and anchoring of GlyRs and $GABA_A$ receptors in cultured neurons (Kasaragod et al. 2019). These interesting but somewhat controversial findings prompted us to explore the effects of artemisinin on inhibitory synapses *in vivo*. We treated young APP-PS1 mice for six weeks with two different doses of artemisinin, and analyzed the expression of gephyrin in the hippocampus, where at this age almost no amyloid plaques are yet developed (Kiss et al. 2016) by Western blot and IF-microscopy. In our previous experiments we disclosed already an increase of key inhibitory synapse proteins in the hippocampus of young APP-PS1 mice in comparison to age matched WTs, probably part of a synaptic compensation process during the very early stages of the disease. Our present findings demonstrated a further increase of gephyrin expression and, unexpectedly, also of gephyrin phosphorylation in artemisinin-treated APP-PS1 mice in comparison to untreated APP-PS1 mice. This elevated gephyrin phosphorylation at the CDK5-dependent site S270, detected with the phospho-specific antibody mAb7a (Kuhse et al. 2012), correlated not only with increased abundancy of $GABA_AR$-γ2 subunits but also elevated levels of the CDK5 regulatory protein p35 (Figure 2).

To prove a functional link between the phosphorylation of gephyrin at this site and the observed changes of $GABA_AR$-γ2 densities – seemingly involved also in the effects of artemisinin on APP-PS1-brains – we performed site-directed mutagenesis experiments with gephyrin expressed in cultured hippocampal neurons. A lentivirus knockdown approach was established and proven to efficiently reduce endogenous gephyrin in these cells (Supplementary Figure 1). The expression of N-terminally myc-tagged gephyrin in the same cells, with more typical gephyrin staining pattern than Eos2-gephyrin was used to examine by confocal IF-microscopy whether mutations at distinct phosphorylation sites have an effect on number, size and intensities of postsynaptic gephyrin-, $GABA_AR$-γ2 – or VIAAT-clusters. In addition to the substitution of Ser270 to alanine, Ser200, a second CDK5 phosphorylation-consensus sequence, was also substituted by alanine codon sequence, alone or in combination with Ser270. Surprisingly, the image analysis of triple immunolabeled (myc, $GABA_AR$-γ2 and VIAAT) cells evidenced similar efficient clustering of wild-type and all three gephyrin mutants within the dendritic and somato-dendritic compartment of cultured hippocampal neurons (DIV15) without a significant change in cluster number. However, the average of IF-intensities measured in the area of overlapping immunoreactivity for all three proteins which should correlate to the relative density of these proteins at these sites disclosed a significant reduction of gephyrin and $GABA_AR$-γ2 subunit density for both single mutants compared to wild-type myc-tagged gephyrin. This result corresponds and is supported by recent findings demonstrating that the reduction of gephyrin phosphorylation at residue Ser270 in spinal cord neurons is associated with a selective increase in $GABA_AR$ diffusion and the loss of the receptors from synapses (Niwa et al. 2019). The density for VIAAT immunoreactivity was not altered significantly, indicating that these gephyrin phosphorylation site-related changes are at least initially limited to the postsynaptic compartment.

To gain further insight into the functional consequences of a site-specific amino acid substitution and thus of the respective gephyrin phosphorylation site *in vitro*, we induced excitatory bursts in cultured hippocampal neurons carrying the site-specific amino acid substitutions by gabazine, a $GABA_AR$ specific inhibitor, and monitored the oscillating activity of neuronal networks using the Ca^{++}-sensor protein hSyn:GCaMP6f.NLS.HA. Comparing the

gabazine-sensitivity of neuronal networks between non-infected cells and cells expressing the wild-type gephyrin or the gephyrin mutant gephyrin^{S270A} we could confirm the capacity of these cells to generate burst activity. In addition we could demonstrate the reduction of the minimal gabazine concentration needed for the induction of a certain frequency of excitatory bursts, indicating a reduced inhibitory drive with gephyrin mutated at Ser270.

In cultures expressing wild-type gephyrin gabazine treatment resulted in a reduction of the postsynaptic IF-intensity of both gephyrin and $GABA_AR$-γ2. This finding coincides with the earlier reported increase in the lateral diffusion of $GABA_A$ receptor γ2 subunits upon increased neuronal activity. In this study the authors used hippocampal neurons at DIV21 and showed that synaptic $GABA_AR$ and endogenous gephyrin cluster fluorescence, which is considered to reflect the number of synaptic receptors and scaffolding proteins, respectively, were reduced when excitatory activity was pharmacologically increased (Bannai et al. 2009).

Our study confirms these data in hippocampal neurons at DIV15 using recombinant myc-tagged gephyrin and additionally provides evidence that the dynamic change at the inhibitory post-synapse is dependent on the phosphorylation of gephyrin at two CDK5-dependent sites, since alanine substitutions at these sites abolished the reduction of gephyrin and $GABA_AR$-γ2 IF-intensities in cells treated with gabazine.

Thus far, several studies demonstrated the significant role of gephyrin phosphorylation for gephyrin clustering and structural and functional plasticity of GABAergic synapses (Battaglia et al. 2018; Herweg and Schwarz 2012; Tyagarajan et al. 2011; Zacchi et al. 2014). One of the first studies proposed that the phosphorylation at gephyrin Ser188, Ser194, and Ser200, has a major functional impact on GlyR cluster formation in cultured spinal cord neurons involving the binding of gephyrin to the chaperone protein PIN1 (Zita et al. 2007). A later study identified Ser270 as phosphorylation site for glycogen synthase kinase 3β (GSK 3β) regulating the number and size of gephyrin clusters (Tyagarajan et al. 2011). Further studies indicated that gephyrin phosphorylation regulates gephyrin microdomain compaction by detecting a reduced number of gephyrin molecules upon expressing gephyrin mutant GFP-gephyrinS270A (Battaglia et al. 2018). Interestingly, phosphorylation by CamKII at Ser325 was shown to be necessary and sufficient to mediate NMDA receptor activity-dependent alteration in gephyrin cluster number and size (Flores et al. 2015).

Studies conducted by our group demonstrated that downregulation of CDK5 or p35 results in reduced gephyrin phosphorylation at Ser270 and $GABA_A$ receptor clustering in cultured hippocampal neurons (Kalbouneh et al. 2014; Kiss et al. 2020). These findings are supported by a study from Specht and coworkers showing that cAMP-dependent signaling reduces gephyrin phosphorylation at residue Ser270 in spinal cord neurons associated with a selective increase in $GABA_AR$ diffusion and the loss of the receptors from synapses (Niwa et al. 2019).

In the present study we demonstrate that two putative phosphorylation sites (Ser270 and Ser200) in the unstructured linker region of gephyrin, may determine synergistically the activity-dependent remodeling of gephyrin and $GABA_A$ receptor density within postsynaptic membrane specializations. These findings support our hypothesis that gephyrin phosphorylation by deregulated CDK5 activity might have an impact in the alterations of synaptic plasticity already early in AD-pathogenesis. However, considering that the knockdown of either CDK5 or p35 (Kalbouneh et al. 2014; Kiss et al. 2020) resulted in a more profound effect on gephyrin and $GABA_A$ receptor clusters, reducing also their number and size, and that in young APP-PS1 mice the increase of p35 and mAb7a immunoreactivity correlated with an increased number of $GABA_A$ receptor clusters (Hollnagel et al. 2019), it is very likely that in addition to gephyrin S270 and S200 other target sites and proteins are also involved in the regulation of the CDK5-dependent cluster formation of gephyrin and $GABA_A$ receptors.

After all, artemisinin increases gephyrin expression and phosphorylation at this site (Ser270) as well as $GABA_AR$-γ2 subunit level in young APP-PS1 mice and this may involve the upregulation of p35/CDK5 signaling. Our earlier findings supporting an augmentation of the GABAergic synaptic system in young APP-PS1 mice thus early in the pathogenesis of AD, might represent compensatory mechanisms to maintain a relative normal function in early AD stages as assumed also by others (Baazaoui and Iqbal 2018; Jackson et al. 2019). This raises the question whether artemisinin might eventually promote endogenous mechanisms of compensation in the AD-brain, which is considered a relevant therapeutic strategy for AD (Jackson et al. 2019). To find an answer, the functional consequences and long term effects of this treatment on synapses *in vivo* has to be carefully evaluated by further studies.

Materials and methods

Construction of expression plasmid

For the expression of gephyrin mutants two different basic constructs were used. In a first set of experiments, a construct harboring the

coding sequence for an N-terminal fusion to the switchable fluorescent protein mEos2 was used, basically as described (Specht et al. 2013). A human synapsin promoter (S) in pFSGW was used to drive the expression of the described gephyrin-constructs (Körber et al. 2012).

After assuring that the large N-terminal fusion domain interfered with gephyrin clustering we inserted in the connecting linker region between Eos2 and gephyrin reading frames the coding sequence for the viral peptide P2 (Körber et al. 2012), allowing a cleavage of the N-terminal EOS protein. The design of the inserted sequence encoded also a short myc-epitope peptide allowing a specific detection of the recombinant gephyrin by anti-myc antibodies.

Construction of the gephyrin-knock-down vector

The sequences coding for shRNAs directed toward the 3′UTR of gephyrin were cloned into pFSGW using the human synapsin promoter to drive EGFP expression as described (Körber et al. 2012).

The gephyrin-shRNA1-Geph-kd-2467-sense target sequence was as follows: ttGTCAACATCTTGAACTATATTgtgaagccacagatgAATATAGTTCAAGATGTTGACttttt and the shRNA2-Geph-kd-2546-sense target sequence was: tttGACAACTCTATTCTGGTTATAgtgaagccacagatgTATAACCAGAATAGAGTTGTCtttt. These sequences were first cloned into the BstBI and BbsI restriction sites of the plasmid pCMV-U6 delBbsI, allowing the subsequent recloning of NheI-BstBI restriction fragments containing the described shRNA sequences under the control of the U6 promotor into the NheI and BstBI sites of pFSGW.

Site-directed mutagenesis

Site-directed mutagenesis of Eos2-gephyrin-P1 clone or myc-gephyrin-coding sequence was performed using the QuickChange Lightning mutagenesis kit from Stratagene (Stratagene, La Jolla, USA) following the supplier's instructions. Mutants were verified by sequence analysis.

Lentivirus preparation

Recombinant lentiviral particles were produced as described previously (Lois et al. 2002). In brief, HEK293LTV cells (Cell Biolabs, San Diego, USA) were transfected with equimolar amounts of pFSGW, pdelta8.9 and pVSVg using polyethyleneimine (Sigma-Aldrich, St. Louis, USA). Virus particles were harvested two days after transfection by collecting the cell culture supernatant and concentrated by ultracentrifugation (90 min at 75,000 *g* in a SW32Ti rotor, Beckman Coulter, Brea, USA). Virus-containing solution was aliquoted, shock frozen in liquid nitrogen and stored at − 80 °C for further use.

Cell culture

Primary cultures of rat hippocampal neurons were prepared from E19 embryos plated at a density of 40,000 cells/cm^2 and infected with lentivirus diluted in medium into 24-well plates (Kiss et al. 2020). Infection with lentivirus dilutions was performed two days after plating (days *in vitro*/DIV2) with lentiviruses expressing either Eos2-gephyrin or rat myc-gephyrin wild-type, or gephyrin mutants with serine residues replaced by alanine by site-directed mutagenesis. Cells were harvested for immunoblotting or fixed for immunocytochemistry at DIV14-15. For details on hippocampal cell cultures and viral infection for Ca^{++}-imaging see the online Supplementary Material.

Animals and tissue preparation

The double transgenic mice on a C57BL/6J genetic background (APP-PS1) used in these experiments co-express the KM670/671NL "Swedish" mutated APP and the L166P-mutation carrying human PS1 under the control of a neuron-specific Thy1 promoter element. Based on the elevated production of human Aβ peptide, the APP-PS1 mouse model mimics aspects of cerebral amyloidosis with amyloid plaque deposition in the hippocampus starting at 4–5 months of age (Radde et al. 2006). Cognitive impairment including deficits in the Morris Water maze test and impairments of LTP in the hippocampal sub-region CA1 were reported starting at 7–8 months of age (Gengler et al. 2010).

APP-PS1 mice were obtained from Prof. Dr. M. Jucker (University of Tübingen, Germany) and bred in the animal unit of the University of Kaiserslautern, Germany. All animal procedures were carried out in accordance with the European Communities Council Directive (86/609/EEC) and approved by the responsible regional state authorities (T-65/15 G-72/17 and 23 177-07/G 18-2-041).

Six weeks old male APP-PS1 mice were randomly assigned to three experimental groups: APP-PS1 (A) mice on chow diet, and two artemisinin-treatment groups, artemisinin being mixed in the chow rodent diet at a dose of 10 and 100 mg/kg, respectively (A-ARM10 and A-ARM100) for further six weeks. The doses for artemisinin were chosen after apprehensive literature research (Ho et al. 2014). At three months of age mice (4–6 animals/group) were deeply anesthetized with isoflurane, brains were dissected and hemispheres separated. For immunohistochemistry, one hemisphere of each brain was mounted in OCT embedding compound (VWR Chemicals, Leuven, Belgium) and snap-frozen in an absolute ethanol-dry ice mixture. For biochemical analysis, fresh hippocampus was dissected from the brain hemispheres and immediately frozen in liquid nitrogen. Tissue samples were stored at −80 °C until use (Kiss et al. 2016).

Protein extracts and immunoblot analysis

Protocols were previously described (Kiss et al. 2016, 2020). Primary antibodies used are indicated in Table 1. After exposure to hyperfilms (Amersham Bioscience, Amersham, Buckinghamshire, United Kingdom), pixel intensities of the bands of interest were analyzed using ImageJ. Band intensities were averaged from three to five animals (hippocampal tissue/group).

Immunolabeling

For brain sections: The protocol was described in details previously (Kiss et al. 2016). Briefly, coronal cryostat sections (8 µm) cut from fresh-frozen brain hemispheres were fixed with 4% (w/v) PFA (ROTI®Histofix 4%) (Carl Roth GmbH, Karlsruhe, Germany) for 8 min and incubated overnight at 4 °C with primary antibodies diluted in blocking solution without Triton X-100 (Table 1). Primary antibodies were detected with corresponding secondary antibodies conjugated to fluorophores (Vector Laboratories, Invitrogen, Jackson Immunoresearch Laboratories). Controls omitting the primary antibodies were

Table 1: Antibodies used in this study.

Primary antibody	Supplier	Species/ Host	Type	Dilution			Catalog number
				IF tissue	IF cells	WB	
p35/p25	Cell Signaling	rabbit	monoclonal	1:200	1:200 1:100	1:1000	C64B10
p35	Abcam	rabbit	polyclonal	1:200			ab64960
p35 (C19)	Santa Cruz Biotechnology	rabbit	polyclonal	1:500			Sc-820
VIAAT	Sigma	rabbit	polyclonal		1:2000		V5764
VGAT	Synaptic Systems	guinea pig	polyclonal		1:1000		131004
γ2-$GABA_A$-R	Synaptic Systems	guinea pig	polyclonal	1:400	1:500		224004
pGephyrin (Ser270) clone mAb7a	Synaptic Systems	mouse	monoclonal	1:200			147011
pGephyrin (Ser270) clone mAb7a	Anatomy and Cell Biology, University of Heidelberg, Germany	mouse	monoclonal		1:200	1:500	Pfeiffer et al. (1984)
Gephyrin (3B11)	Synaptic Systems, Göttingen, Germany	mouse	monoclonal			1:20.000	147111
hAPP	Millipore	mouse	monoclonal			1:5000	MABN10
myc (9E10)	Invitrogen	mouse	polyclonal		1:1000		MA1-980
β–actin	Sigma	mouse	monoclonal			1:40.000	A5441

included. Serial sections from untreated and treated APP-PS1 mice were labeled simultaneously using the same batches of solutions to avoid differences in immunolabeling conditions.

For cultured hippocampal neurons: The protocol was previously described previously (Kiss et al. 2020). Briefly, coverslips containing cultured neurons at DIV15 were washed once with PBS and subsequently fixed with 4% (w/v) PFA for 10 min at RT. After blocking with 5% horse-serum and 1% BSA solution containing 0.1% Triton X-100 (Roth) for 30 min cells were incubated with up to three primary antibodies (Table 1) overnight at 4 °C followed on the next day by incubation with appropriate secondary antibodies conjugated to fluorophores (Vector Laboratories, Invitrogen, Jackson Immunoresearch Laboratories, West Grove, USA) for 30 min at room temperature.

Confocal laser scanning microscopy and quantitative IF-analysis

Images were captured with a Leica TCS SP8 microscope (Leica Microsystems CMS GmbH, Mannheim, Germany) using an HC PL APO CS2 63.0 × 1.40 oil objective or a 63×/1.46 oil objective.

For brain sections: The protocol was described in detail previously (Kiss et al. 2016, 2020). The images were acquired in sequential mode with a frame average of four stacks of eight optical sections (1024 × 1024 pixels) spaced by 500 nm. Laser power and settings were identical for all samples in an experiment. Three randomly chosen fields within CA1 and DG of each hippocampus (n = 3–6 brains/group) were recorded for quantitative analysis. In each field, rectangular areas of 500 × 150 µm within the pyramidal cell layer (PCL) and stratum radiatum (SR) of CA1 and the granular cell layer (GCL) of DG were randomly selected and quantified for mean fluorescence intensities using NIH's Fiji (pacific.mpi-cbg.de/wiki/index.php/fiji). Mean fluorescence intensity of a region of interest was calculated from maximal intensity projection of eight optical sections. Mean values calculated for each animal were used for final statistics. Mean values of untreated APP-PS1 mice were set to one, and data are given as mean ± SEM.

For hippocampal neurons: The images were acquired using a Zeiss Axio Observer fluorescence microscope (63×/1.46 oil objective) with two-fold electronic zoom in sequential mode with a frame average of two stacks of five optical sections. Laser power and settings were identical for all samples and experiments for each channel. Neurons of similar size and morphology were chosen using the green channel (myc-gephyrin) without knowledge of fluorescence intensities of the red channel ($GABA_A$R-γ2) and images of proximal dendritic areas (n = 5–10 neurons/experiment) were recorded and maximum intensity projections were used for quantitative analysis. To analyze fluorescence intensities at overlapping sites for myc-gephyrin, $GABA_A$R-γ2 and VIAAT in the triple-labeled hippocampal neurons an ImageJ/Fiji macro was developed (CellNetworks Math-Clinic Core Facility, University of Heidelberg, Germany) as described (Hollnagel et al. 2019). This first semi-automatically segmented the immunofluorescent puncta using the threshold method and then automatically processed the generated binary masks to find overlapping signals between the three different confocal channels. The number and area of overlapping puncta and corresponding fluorescence intensities for each channel were then counted by the ImageJ/Fiji macro and a customized summary table was created in the output directory for each processed image for further validation and statistical analysis. Mean values calculated for each neuron were used for statistical analysis (25 neurons/group from four independent cultures and 25–40/group from three independent cultures). In addition, single channel images were also analyzed separately with ImageJ/Fiji using the same threshold settings determined manually for all images of one experiment (wt compared to mutants).

Statistical analysis

Statistical evaluation was done in Prism (GraphPad Software Inc). Statistical significance of IF and immunoblot data were determined

using unpaired Student's *t*-test: $*p < 0.05$, $**p < 0.01$ and $***p < 0.001$ or ordinary one-way ANOVA with post-hoc test (Tukey's or Bonferroni multiple comparison-test). Numeric values are given as mean ± SEM or standard deviation (SD) or as medians with box-plots as specified.

Acknowledgments: We thank Dagmar Groß (Department of Human Biology and Human Genetics, University of Kaiserslautern, Germany) and Rita Rosner (Department of Anatomy and Cell Biology, University of Heidelberg, Germany) for excellent technical assistance, H. Eckehard Freitag, Thomas Lissek, and Anna M. Hagenston for generating a viral expression vector encoding a nuclear-targeted version of GCaMP6f and for providing recombinant adeno-associated virus, Natalia Schichta for excellent image analysis, and Dr. Carlo Antonio Beretta (CellNetworks Math-Clinic Core Facility at Heidelberg, University of Heidelberg, Germany) for developing ImageJ/Fiji macro.

Author contributions: All the authors have accepted responsibility for the entire content of this submitted manuscript and approved submission.

Research funding: This work was supported by a grant of Romanian Ministry of Research and Innovation CNCS-UEFISCDI (PN-III-P4-ID-PCE-2016-0052, within PNCDI III) to E.K. and a grant of the Alzheimer Forschung Initiative e.V. (AFI) (Project number: 17024) to J.K., E.K. and S.K.

Conflict of interest statement: The authors declare no conflicts of interest regarding this article.

References

Arnold, F.J., Hofmann, F., Bengtson, C.P., Wittmann, M., Vanhoutte, P., and Bading, H. (2005). Microelectrode array recordings of cultured hippocampal networks reveal a simple model for transcription and protein synthesis-dependent plasticity. J. Physiol. 564: 3–19.

Baazaoui, N., and Iqbal, K. (2018). A novel therapeutic approach to treat Alzheimer's disease by neurotrophic support during the period of synaptic compensation. J. Alzheim. Dis. 62: 1211–1218.

Bannai, H., Lévi, S., Schweizer, C., Inoue, T., Launey, T., Racine, V., Sibarita, J.B., Mikoshiba, K., and Triller, A. (2009). Activity-dependent tuning of inhibitory neurotransmission based on GABAAR diffusion dynamics. Neuron 62: 670–682.

Battaglia, S., Renner, M., Russeau, M., Côme, E., Tyagarajan, S.K., and Lévi, S. (2018). Activity-dependent inhibitory synapse scaling is determined by gephyrin phosphorylation and subsequent regulation of GABAA receptor diffusion. eNeuro 5: ENEURO.0203-17.2017.

Calvo-Flores Guzmán, B., Vinnakota, C., Govindpani, K., Waldvogel, H.J., Faull, R., and Kwakowsky, A. (2018). The GABAergic system as a therapeutic target for Alzheimer's disease. J. Neurochem. 146: 649–669.

Flores, C.E., Nikonenko, I., Mendez, P., Fritschy, J.M., Tyagarajan, S.K., and Muller, D. (2015). Activity-dependent inhibitory synapse remodeling through gephyrin phosphorylation. Proc. Natl. Acad. Sci. U.S.A. 112: E65–E72.

Frozza, R.L., Lourenco, M.V., and De Felice, F.G. (2018). Challenges for Alzheimer's disease therapy: insights from novel mechanisms beyond memory defects. Front. Neurosci. 12: 37.

Gengler, S., Hamilton, A., and Hölscher, C. (2010). Synaptic plasticity in the hippocampus of a APP/PS1 mouse model of Alzheimer's disease is impaired in old but not young mice. PloS One 5: e9764.

Groeneweg, F.L., Trattnig, C., Kuhse, J., Nawrotzki, R.A., and Kirsch, J. (2018). Gephyrin: a key regulatory protein of inhibitory synapses and beyond. Histochem. Cell Biol. 150: 489–508.

Hawasli, A.H., Benavides, D.R., Nguyen, C., Kansy, J.W., Hayashi, K., Chambon, P., Greengard, P., Powell, C.M., Cooper, D.C., and Bibb, J.A. (2007). Cyclin-dependent kinase 5 governs learning and synaptic plasticity via control of NMDAR degradation. Nat. Neurosci. 10: 880–886.

Herweg, J., and Schwarz, G. (2012). Splice-specific glycine receptor binding, folding, and phosphorylation of the scaffolding protein gephyrin. J. Biol. Chem. 287: 12645–12656.

Ho, W.E., Peh, H.Y., Chan, T.K., and Wong, W.S. (2014). Artemisinins: pharmacological actions beyond anti-malarial. Pharmacol. Ther. 142: 126–139.

Hollnagel, J.O., Elzoheiry, S., Gorgas, K., Kins, S., Beretta, C.A., Kirsch, J., Kuhse, J., Kann, O., and Kiss, E. (2019). Early alterations in hippocampal perisomatic GABAergic synapses and network oscillations in a mouse model of Alzheimer's disease amyloidosis. PloS One 14: e0209228.

Jackson, J., Jambrina, E., Li, J., Marston, H., Menzies, F., Phillips, K., and Gilmour, G. (2019). Targeting the synapse in Alzheimer's disease. Front. Neurosci. 13: 735.

Kalbouneh, H. (2013). *The functional consequences of gephyrin phosphorylation by Cdk5 on inhibitory synapses*, Dissertation. Heidelberg, Germany, Heidelberg University.

Kalbouneh, H., Schlicksupp, A., Kirsch, J., and Kuhse, J. (2014). Cyclin-dependent kinase 5 is involved in the phosphorylation of gephyrin and clustering of GABAA receptors at inhibitory synapses of hippocampal neurons. PloS One 9: e104256.

Kasaragod, V.B., Hausrat, T.J., Schaefer, N., Kuhn, M., Christensen, N.R., Tessmer, I., Maric, H.M., Madsen, K.L., Sotriffer, C., Villmann, C., et al. (2019). Elucidating the molecular basis for inhibitory neurotransmission regulation by artemisinins. Neuron 101: 673–689.

Kim, E.Y., Schrader, N., Smolinsky, B., Bedet, C., Vannier, C., Schwarz, G., and Schindelin, H. (2006). Deciphering the structural framework of glycine receptor anchoring by gephyrin. EMBO J. 25: 1385–1395.

Kim, S.H., and Ryan, T.A. (2010). CDK5 serves as a major control point in neurotransmitter release. Neuron 67: 797–809.

Kiss, E., Gorgas, K., Schlicksupp, A., Groß, D., Kins, S., Kirsch, J., and Kuhse, J. (2016). Biphasic alteration of the inhibitory synapse scaffold protein gephyrin in early and late stages of an Alzheimer disease model. Am. J. Pathol. 186: 2279–2291.

Kiss, E., Groeneweg, F., Gorgas, K., Schlicksupp, A., Kins, S., Kirsch, J., and Kuhse, J. (2020). Amyloid-β fosters p35/CDK5 signaling contributing to changes of inhibitory synapses in early stages of cerebral amyloidosis. J. Alzheimers Dis. 74: 1167–1187.

Kneussel, M., Brandstätter, J.H., Laube, B., Stahl, S., Müller, U., and Betz, H. (1999). Loss of postsynaptic GABA(A) receptor clustering in gephyrin-deficient mice. J. Neurosci. 19: 9289–9297.

Körber, C., Richter, A., Kaiser, M., Schlicksupp, A., Mükusch, S., Kuner, T., Kirsch, J., and Kuhse, J. (2012). Effects of distinct collybistin isoforms on the formation of GABAergic synapses in hippocampal neurons. Mol. Cell. Neurosci. 50: 250–259.

Kuhse, J., Kalbouneh, H., Schlicksupp, A., Mükusch, S., Nawrotzki, R., and Kirsch, J. (2012). Phosphorylation of gephyrin in hippocampal neurons by cyclin-dependent kinase CDK5 at Ser-270 is dependent on collybistin. J. Biol. Chem. 287: 30952–30966.

Kwakowsky, A., Calvo-Flores Guzmán, B., Govindpani, K., Waldvogel, H.J., and Faull, R.L. (2018). Gamma-aminobutyric acid A receptors in Alzheimer's disease: highly localized remodeling of a complex and diverse signaling pathway. Neural Regen. Res. 13: 1362–1363.

Li, J., Casteels, T., Frogne, T., Ingvorsen, C., Honoré, C., Courtney, M., Huber, K.V.M., Schmitner, N., Kimmel, R.A., Romanov, R.A., et al. (2017). Artemisinins target GABAA receptor signaling and impair α cell identity. Cell 168: 86–100.

Li, S., Zhao, X., Lazarovici, P., and Zheng, W. (2019). Artemether activation of AMPK/GSK3β(ser9)/Nrf2 signaling confers neuroprotection towards β-amyloid-induced neurotoxicity in 3xTg Alzheimer's mouse model. Oxid. Med. Cell. Longev. 21: 1862437.

Liang, J., López-Valdés, H.E., Martínez-Coria, H., Lindemeyer, A.K., Shen, Y., Shao, X.M., and Olsen, R.W. (2014). Dihydromyricetin ameliorates behavioral deficits and reverses neuropathology of transgenic mouse models of Alzheimer's disease. Neurochem. Res. 39: 1171–1181.

Liu, S.L., Wang, C., Jiang, T., Tan, L., Xing, A., and Yu, J.T. (2016). The role of Cdk5 in Alzheimer's disease. Mol. Neurobiol. 53: 4328–4342.

Lois, C., Hong, E.J., Pease, S., Brown, E.J., and Baltimore, D. (2002). Germline transmission and tissue-specific expression of transgenes delivered by lentiviral vectors. Science 295: 868–872.

Lu, B.W., Baum, L., So, K.F., Chiu, K., and Xie, L.K. (2019). More than anti-malarial agents: therapeutic potential of artemisinins in neurodegeneration. Neural Regen. Res. 14: 1494–1498.

Maric, H.M., Mukherjee, J., Tretter, V., Moss, S.J., and Schindelin, H. (2011). Gephyrin-mediated γ-aminobutyric acid type A and glycine receptor clustering relies on a common binding site. J. Biol. Chem. 286: 42105–42114.

Mishiba, T., Tanaka, M., Mita, N., He, X., Sasamoto, K., Itohara, S., and Ohshima, T. (2014). Cdk5/p35 functions as a crucial regulator of spatial learning and memory. Mol. Brain 7: 82.

Mita, N., He, X., Sasamoto, K., Mishiba, T., and Ohshima, T. (2016). Cyclin-dependent kinase 5 regulates dendritic spine formation and maintenance of cortical neuron in the mouse brain. Cerebr. Cortex 26: 967–976.

Morabito, M.A., Sheng, M., and Tsai, L.H. (2004). Cyclin-dependent kinase 5 phosphorylates the N-terminal domain of the postsynaptic density protein PSD-95 in neurons. J. Neurosci. 24: 865–876.

Niwa, F., Patrizio, A., Triller, A., and Specht, C.G. (2019). cAMP-EPAC-dependent regulation of gephyrin phosphorylation and GABAAR trapping at inhibitory synapses. iScience 22: 453–465.

Okorji, U.P., Velagapudi, R., El-Bakoush, A., Fiebich, B.L., and Olajide, O.A. (2016). Antimalarial drug artemether inhibits neuroinflammation in BV2 microglia through Nrf2-dependent mechanisms. Mol. Neurobiol. 53: 6426–6443.

Pfeiffer, F., Simler, R., Grenningloh, G., and Betz, H. (1984). Monoclonal antibodies and peptide mapping reveal structural similarities between the subunits of the glycine receptor of rat spinal cord. Proc. Natl. Acad. Sci. U.S.A. 81: 7224–7227.

Prior, P., Schmitt, B., Grenningloh, G., Pribilla, I., Multhaup, G., Beyreuther, K., Maulet, Y., Werner, P., Langosch, D., Kirsch, J., et al. (1992). Primary structure and alternative splice variants of gephyrin, a putative glycine receptor-tubulin linker protein. Neuron 8: 1161–1170.

Qiang, W., Cai, W., Yang, Q., Yang, L., Dai, Y., Zhao, Z., Yin, J., Li, Y., Li, Q., Wang, Y., et al. (2018). Artemisinin B improves learning and memory impairment in AD dementia mice by suppressing neuroinflammation. Neuroscience 395: 1–12.

Radde, R., Bolmont, T., Kaeser, A., Coomaraswamy, J., Lindau, D., Stoltze, L., Calhoun, M.E., Jäggi, F., Wolburg, H., Gengler, S., et al. (2006). Abeta42-driven cerebral amyloidosis in transgenic mice reveals early and robust pathology. EMBO Rep. 7: 940–946.

Saiyed, T., Paarmann, I., Schmitt, B., Haeger, S., Sola, M., Schmalzing, G., Weissenhorn, W., and Betz, H. (2007). Molecular basis of gephyrin clustering at inhibitory synapses: role of G- and E-domain interactions. J. Biol. Chem. 282: 5625–5632.

Selkoe, D.J., and Hardy, J. (2016). The amyloid hypothesis of Alzheimer's disease at 25 years. EMBO Mol. Med. 8: 595–608.

Seo, E.J., Fischer, N., and Efferth, T. (2018). Phytochemicals as inhibitors of NF-κB for treatment of Alzheimer's disease. Pharmacol. Res. 129: 262–273.

Shi, J.Q., Zhang, C.C., Sun, X.L., Cheng, X.X., Wang, J.B., Zhang, Y.D., Xu, J., and Zou, H.Q. (2013). Antimalarial drug artemisinin extenuates amyloidogenesis and neuroinflammation in APPswe/PS1dE9 transgenic mice via inhibition of nuclear factor-κB and NLRP3 inflammasome activation. CNS Neurosci. Ther. 19: 262–268.

Shupp, A., Casimiro, M.C., and Pestell, R.G. (2017). Biological functions of CDK5 and potential CDK5 targeted clinical treatments. Oncotarget 8: 17373–17382.

Specht, C.G., Izeddin, I., Rodriguez, P.C., El Beheiry, M., Rostaing, P., Darzacq, X., Dahan, M., and Triller, A. (2013). Quantitative nanoscopy of inhibitory synapses: counting gephyrin molecules and receptor binding sites. Neuron 79: 308–321.

Tyagarajan, S.K., Ghosh, H., Yévenes, G.E., Nikonenko, I., Ebeling, C., Schwerdel, C., Sidler, C., Zeilhofer, H.U., Gerrits, B., Muller, D., et al. (2011). Regulation of GABAergic synapse formation and plasticity by GSK3β-dependent phosphorylation of gephyrin. Proc. Natl. Acad. Sci. U.S.A. 108: 379–384.

Vico Varela, E., Etter, G., and Williams, S. (2019). Excitatory-inhibitory imbalance in Alzheimer's disease and therapeutic significance. Neurobiol. Dis. 127: 605–615.

Zacchi, P., Antonelli, R., and Cherubini, E. (2014). Gephyrin phosphorylation in the functional organization and plasticity of GABAergic synapses. Front. Cell. Neurosci. 8: 103.

Zhao, X., Li, S., Gaur, U., and Zheng, W. (2020). Artemisinin improved neuronal functions in Alzheimer's disease animal model 3xtg

mice and neuronal cells via stimulating the ERK/CREB signaling pathway. Aging Dis. 11: 801–819.

Zita, M.M., Marchionni, I., Bottos, E., Righi, M., Del Sal, G., Cherubini, E., and Zacchi, P. (2007). Post-phosphorylation prolyl isomerisation of gephyrin represents a mechanism to modulate glycine receptors function. EMBO J. 26: 1761–1771.

Zott, B., Busche, M.A., Sperling, R.A., and Konnerth, A. (2018). What happens with the circuit in Alzheimer's disease in mice and humans? Annu. Rev. Neurosci. 41: 277–297.

Supplementary Material: The online version of this article offers supplementary material (https://doi.org/10.1515/hsz-2021-0153).